Journal of Power Sources 225 (2013) 293–303

Contents lists available at SciVerse ScienceDirect

Journal of Power Sources

journal homepage: www.elsevier.com/locate/jpowsour

Influence of the composition of isopropyl alcohol/water mixture solvents in catalyst ink solutions on proton exchange membrane fuel cell performance

Trung Truc Ngo [a], T. Leon Yu [a,b,*], Hsiu-Li Lin [a,b]

[a] Department of Chemical Engineering & Materials Science, Yuan Ze University, Chung-Li, Taoyuan 32003, Taiwan
[b] Fuel Cell Center, Yuan Ze University, Chung-Li, Taoyuan 32003, Taiwan

HIGHLIGHTS

- Pt surface area increases with decreasing IPA content of catalyst solution.
- Fuel cell performance increases with decreasing IPA content of catalyst solution.
- Pt surface area depends on solubility parameter of catalyst ink solvent.

GRAPHICAL ABSTRACT

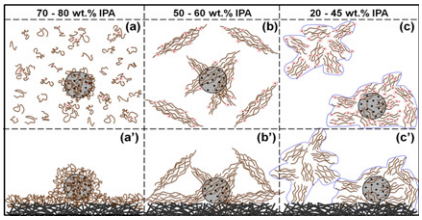

ARTICLE INFO

Article history:
Received 2 September 2012
Received in revised form
12 October 2012
Accepted 15 October 2012
Available online 26 October 2012

Keywords:
Nafion morphology
Nafion dilute solutions
Platinum catalyst electrodes
Membrane electrode assembly
Proton exchange membrane fuel cell

ABSTRACT

We study the morphology of Nafion in the dilute IPA (isopropyl alcohol)/water mixture solutions containing 20–100 wt.% of IPA and in the Pt–C/Nafion gas diffusion electrodes (GDEs; where Pt–C is the carbon powder deposited on its surface with Pt particles), which are prepared by spraying on the carbon paper surfaces with a layer of Pt–C, Nafion and IPA/water ink solution. The fuel cell performance of the GDEs strongly depends on the Nafion morphology in the ink solutions. A lower IPA content in the Pt–C/Nafion ink solutions results in the formation of larger and higher negatively charged Nafion aggregated particles, which leads to higher steric hindrance of the deposition of Nafion ionomer on the surface of Pt–C particles and thus a thinner Nafion film in contact on the Pt–C particle surfaces. The thinner Nafion film in contact with the Pt particles in the CL increases the chances of the Pt particles in contact with the H_2/O_2 gas, leading to a higher fuel cell performance.

1. Introduction

Nafion (a trade name of Du Pont) is an ionomer with a chemical structure that consists of a hydrophobic perfluorocarbon backbone ($-[(CF_2-CF_2)_x-(CF_2-CF)_y]-$) and hydrophilic sulfonated vinylether side chains ($-OCF_2-CF(CF_3)-O-CF_2-SO_3H$) [1–4]. It is an indispensable part of the proton exchange membrane (PEM) and a component of the catalyst ink solutions used in fabricating the membrane electrode assemblies (MEAs) of proton exchange membrane fuel cells (PEMFCs) [5,6]. A high-performance MEA requires a combination of effective contact at the three-phase boundary, high Pt (platinum) catalyst utilization, good proton conduction, and facile H_2 and O_2 reactants and water product transport to and from Pt active sites in the catalyst layer (CL). A Nafion ionomer in the CL helps to increase the three-dimensional zone of catalytic activity. Nafion serves as the physical binder and proton conductor in the CLs and facilitates the molecular interaction among the Pt particles; the Nafion ionomer may also play a key role in determining the final microstructure and properties of the CLs [7]. The catalyst ink solutions for MEA fabrications consist of Pt–C (Pt on a carbon powder support), the Nafion ionomer, and solvents. The molecular interactions of the Nafion ionomer and the

* Corresponding author. Department of Chemical Engineering & Materials Science, Yuan Ze University, Chung-Li, Taoyuan 32003, Taiwan. Tel.: +886 3 4638800x2553; fax: +886 3 4559373.
E-mail address: cetlyu@saturn.yzu.edu.tw (T.L. Yu).

0378-7753/$ – see front matter © 2012 Elsevier B.V. All rights reserved.
http://dx.doi.org/10.1016/j.jpowsour.2012.10.055

solvents control the Nafion molecular conformations in the solutions and thus the final microstructure of Nafion in the CLs. Thus, it is important to understand the Nafion solution properties to obtain a high performance MEA.

Several studies have been devoted to the properties of Nafion solutions as well as the morphology of Nafion ionomers in dilute solutions containing various solvents [8–18]. Alcohol/water mixture solvents, especially isopropyl alcohol (IPA) and water mixtures, are the most common solvents used in preparing catalyst ink solutions. The structures of Nafion ionomers in water and methyl alcohols have been investigated using small angle neutron scattering (SANS), small angle X-ray scattering (SAXS), and electron spin resonance (ESR) for Nafion concentrations ranging from 1 to 22 wt.% [8–13]. The results showed that Nafion hydrophobic perfluorocarbon backbones aggregated and formed compact cylinders in solvents, with the hydrophilic sulfonated vinylether side chains surrounding the surfaces of the aggregated cylinders and in contact with the solvents. Dynamic light scattering (DLS) investigations have been carried out in dilute Nafion/ethanol–water (ethanol/water = 50/50 vol ratio) [14], Nafion/water [15], and Nafion/methanol–water (methanol/water = 4/1 wt. ratio) solutions [16]. Two modes of Nafion particle size distribution were found. The authors attributed these two aggregates to the hydrophobic inter-polymer fluorocarbon backbone interactions and the hydrophilic inter-polymer vinylether sulfonic acidic ion pair interactions. The morphology of commercial Nafion membranes has also been investigated using SAXS and SANS [18–31], wide angle X-ray diffraction [20,24,25,28], atomic force microscopy [30,31], and electron microscopy [30,31]. The SAXS and SANS data reveal that the Nafion membranes are composed assemblies of bundles of fibrils, which correspond to elongated polymeric aggregates surrounded with ionic charges. Most of the commercial Nafion membranes were obtained from Du Pont Co. and were prepared by extrusion. Few studies in the literature have reported on the molecular morphology of Nafion solution casting membranes and CLs fabricated using Nafion/Pt–C ink solutions. The influence of solvents of the Pt–C/Nafion catalyst ink solutions on the Nafion thin film morphology of CLs and on the fuel cell performance is still not clear to us.

There are three CL processing methods, i.e., decal method [32], gas diffusion layer (GDL)-based method [33], and membrane-based or catalyst-coated membrane (CCM) method [34] have been reported in literature. Uchida et al. [33] and Shin et al. [35] prepared electrodes using GDL-based method and reported that the dielectric constant ε of solvent used for the Pt–C/Nafion catalyst ink solutions determines the state of the Nafion ionomer in the solutions. Depending on the ε value, the Nafion solvent mixture can be in the form of solution ($\varepsilon > 10$), colloids ($10 > \varepsilon > 3$), and precipitates ($\varepsilon < 3$). Fuel cell performance and electrochemical analyses revealed that the electrode prepared by a colloidal method had a better results compared to those of the solution method. These authors mentioned that the colloidal method appeared to secure continuity of the ionomer network and higher porosity in the CL, resulting in higher proton conductivity, less mass transfer resistance, and higher fuel cell performance. The effect of the organic solvents with various εs, including isopropyl alcohol, ethanol, methanol, amyl alcohol, acetone, ethylene glycol, 1,2 propylene glycol, 1,3 propylene glycol, diethyl oxalate, dimethyl ether, ethylene glycol diethyl ether, water/ethylene glycol mixture, butyl acetate/glycerol mixture, ethanol/glycerol mixture, isopropyl alcohol/glycerol mixture, water/glycerol mixture etc., on the structure of CLs and the fuel cell performance of MEAs were further studied by using decal [36,37], GDL-based [38,39], and CCM [40] processing methods. All these papers discussed the morphology of CLs and the fuel cell performance of MEAs based on the ε value of the solvent of catalyst ink solutions.

Nafion has been reported to possess dual solubility parameters δs, i.e. $\delta_1 = 9.7$ cal$^{0.5}$ cm$^{-1.5}$ for the perfluorocarbon backbone and $\delta_2 = 17.3$ cal$^{0.5}$ cm$^{-1.5}$ for the sulfonated vinylether side chains [41]. In previous work [16–18], we showed the morphology of Nafion ionomer in the dilute solutions and in the solution casting membranes depends not only on the ε but also on the δ of the solvents. However, the study of the influence of δ of the solvent of catalyst ink solution on the morphology of Nafion ionomer in CLs and the fuel cell performance have not been reported in literature. Alcohol/water mixture solvents, especially isopropyl alcohol (IPA) and water mixtures, are the most common solvents used in preparing catalyst ink solutions. The physical properties of Nafion in IPA/water mixture solutions as a function of their compositions have rarely been investigated and discussed; thus, the optimum IPA/water wt. ratio of the catalyst ink solutions for the MEA CL fabrication remains unclear. In this work, we examine how the composition of the IPA/water mixture solvents influences the morphology of Nafion molecules in the solutions, the properties of the Pt–C/Nafion (where Pt–C is the carbon powder with 38 wt.% Pt particles deposited on its surface) catalyst ink solutions, and the Pt–C/Nafion microstructures of the CLs prepared by using GDL-based method. The morphology of Nafion ionomers in the IPA/water mixture solutions with various IPA concentrations ($\varepsilon > 10$) is observed and discussed based on the inter-molecular hydrogen bonding, εs, and δs of the mixture solvents. The results were correlated with the Pt electrochemical active surface areas (ECSAs) of the CLs and their performance in fuel cells, in an attempt to correlate the composition of the IPA/water mixture solvent of the Pt–C/Nafion ink solutions with the Pt ECSAs in the CLs and with the fuel cell performance. The main purpose of this study is to find the optimum IPA/water composition of the Pt–C/Nafion ink solutions for CL fabrication and MEA preparation.

2. Experimental

2.1. Viscosity of IPA/water mixture solvents

The flow times of the IPA (reagent grade, J.T. Baker)/water mixture solutions with the IPA concentration varied from 0.0 wt.% to 100.0 wt.% were measured at 25 °C using an Ubbelohde viscometer. The viscosity of each mixture solution was calculated from its flow time, using the viscosity of pure water (i.e., 0.890 cP at 25 °C) as reference [42]. The data were averaged over 3 measurements.

2.2. Nafion solutions preparation

A commercial Nafion solution (Du Pont Co., sulfonic acid equivalent weight of Nafion = ~1100 g equiv^{-1}) containing 20 wt.% of Nafion and 80 wt.% of aliphatic alcohol and water mixture solvent was heated at 60 °C (below T_g = ~105 °C of Nafion) under ambient pressure for 1 h and then at 60 °C under vacuum for 48 h to obtain a solid Nafion resin. The solid Nafion resin was then dissolved in a series of IPA/water mixture solvents, in which the IPA concentration was varied from 20 wt.% to 100 wt.%, to prepare Nafion solutions. A total of 9 Nafion solutions (in which the solvent compositions were [IPA]/[IPA + water] = 100, 80, 70, 60, 55, 50, 45, 40, and 20 wt.%) were prepared. All of the solutions had a Nafion concentration of 0.6 mg mL^{-1}.

2.3. Dynamic light scattering (DLS) of dilute Nafion solutions

DLS hydrodynamic radius (R_h) distribution measurements of 0.6 mg mL^{-1} Nafion in IPA/water mixture solutions with various IPA concentrations were carried out with a 256-channel autocorrelator (model BI9000, Brookhaven Co.) at 25 °C. An Ar ion laser

(wavelength of 514 nm, operated at 100 mW, Spectra Physics) was used, and the scattering angle was $\theta = 60^{\circ}$.

2.4. Transmission electron microscope (TEM) observations

The morphology of Nafion molecules in dilute solutions was observed using a JEM-2100 (HR) TEM at an accelerating voltage of 80 kV. The sample of each Nafion solution prepared as described in Section 2.2 was freeze dried on a copper grid with a 200-mesh carbon film (CF200-Cu, Electron Microscopy Sciences, Inc., PA) sample holder to fix the morphology of the Nafion molecules similarly to that in the dilute solution. The copper grid was floated on the top surface of a drop of 0.6 mg mL^{-1} Nafion solution for 12 h. Thus, a thin film of Nafion solution covered the surface of the copper grid. The copper grid with the thin film of Nafion solution was immediately frozen in a liquid nitrogen container at −190 °C for 4 h. The solvent of the frozen Nafion thin film on the copper grid surface was dried under vacuum at −130 °C for 5 h. The copper grid with the dried Nafion film on its surface was then immersed in a 0.5 M $Pb(NO_3)_2$ (Aldrich Chemical Co.) aqueous solution for 10 min to stain the sulfonic acid groups of Nafion and dried at room temperature. The copper grid was then rinsed with deionized water to clean the residual $Pb(NO_3)_2$ and dried at room temperature.

2.5. Catalyst ink solution preparation

The same solid Nafion resin prepared as described in Section 2.2 was used for the preparation of catalyst ink solutions. The Pt–C catalyst (38 wt.% Pt content, Johnson Matthey), Nafion, and IPA/water mixture solvents with IPA concentrations ranging from 20 wt.% to 80 wt.% were mixed by sonication for at least 48 h at room temperature to obtain homogeneous ink solutions. The wt. ratio of Pt–C/Nafion was 2.3/1, and the concentration of [Pt–C + Nafion] in each ink solution was ~1.0 wt.%. A total of 8 catalyst ink solutions were prepared.

2.6. Pt-ECSA measurements for Pt–C/Nafion gas diffusion electrodes (GDEs)

The catalyst ink solutions containing various concentrations of IPA prepared as described in Section 2.5 were used to prepare Pt–C/Nafion GDE samples by spraying each Pt–C/Nafion ink solution onto a 2 × 1 cm^2 gas diffusion layer (GDL; 10BC carbon papers, SGL Co.) using an ultrasonic spray coating system (Sono Tek Co., NY). After fabrication, the GDE with a CL on its surface was air-dried at ~80 °C for 2 h and then at ~80 °C under vacuum for 30 min. The final wt. ratio of [Pt–C]/[Nafion solid resin] on the GDE was ~2.3/1. The Pt loading for each sample was 0.1 mg cm^{-2}. ECSA measurements were performed using a three-electrode system. A saturated calomel electrode (SCE) was used as a reference electrode, platinum wire as a counter electrode, and the GDE as a working electrode. The measurements were carried out in a 0.5 M H_2SO_4 solution using cyclic voltammetry (CV; CHI611C Electrochemical Analyzer, CH Instruments) with a scan rate of 50 mV s^{-1} versus a normal hydrogen electrode (NHE) at 25 °C. During testing, the working electrode was fed with humidified N_2 at 40 psi of pressure. The specific ECSA was calculated using the following equation [43,44]:

$$\mathrm{ECSA} = Q_H/(m \times q_H) \quad (1)$$

where Q_H is the charge exchanged during the electro-adsorption of H_2 on Pt, m the amount of Pt loading, and q_H (210 mC cm^{-2}) the charge required for monolayer adsorption of H_2 on Pt surfaces.

2.7. Field emission scanning electron microscopy (FESEM) of Pt–C/Nafion GDEs

The same samples prepared in Section 2.6 for Pt-ECSA measurements were used for the FESEM observations, which were performed with JEOL model JSM-6701F, operated at 10 kV.

2.8. MEA preparation

Nafion-212 membranes (Du Pont) were used to fabricate MEAs. Before MEA preparation, the Nafion-212 membrane was treated at 85 °C in 5 wt.% H_2O_2 aqueous solution for 1 h, followed by treatment in distilled water for 1 h, in 0.5 M H_2SO_4 solution at 85 °C for 1 h, and subsequently, in distilled water for 15 min. Eight Pt–C/Nafion catalyst ink solutions with the IPA/water mixture solvents containing 20, 40, 45, 50, 55, 60, 70, and 80 wt.% IPA were used for anode and cathode CL fabrications. The fabrication procedures were same as those used in preparing ECSA measurement samples as described above. The active area of each electrode was 3.5 × 3.5 cm^2. The final wt. ratio of [Pt–C]/[Nafion solid resin] on the GDL was ~2.3/1; the Pt loadings on the anode and cathode CLs were 0.2 mg cm^{-2} and 0.4 mg cm^{-2}, respectively. The Nafion-212 membrane was sandwiched between the anode and cathode electrodes and hot pressed at 50 kg cm^{-2} at 130 °C for 30 s and then at 100 kg cm^{-2} for 60 s. A total of eight MEAs were prepared in this work.

2.9. Unit fuel cell tests and impedance measurements

The performances of the PEMFC unit cells of MEAs prepared as described above (MEA preparations) were tested under ambient pressure using a Model 850e Fuel Cell Test System (Scribner Associates, Inc.). The anode, cathode, and cell temperatures were all 80 °C. The input H_2 and O_2 flow rates were both 500 mL min^{-1} with 100% RH. The cell was activated at 80 °C and at a constant voltage of 0.6 V for 10 min and then at open circuit for 3 min; subsequently, at a constant voltage of 0.4 V for 10 min and then at open circuit for 3 min to enhance humidification and activation of the MEA. The above activation procedure was repeated for at least 17 cycles before each i–V curve measurement was carried out. The i–V curves were obtained by measuring the current density i with the step decrement of voltage at an interval of 0.05 V; each measurement lasted for 30 s. The impedances of the MEAs were measured using the same fuel cell test system. The frequency response analyzer was a Model 850e Fuel Cell Test System (Scribner Associates, Inc.). The potential state was kept at i = 1000 mA cm^{-2}, and the scanning frequency was from 10^4 Hz to 0.1 Hz.

3. Results and discussion

3.1. Densities and viscosities of IPA/water mixture solvents

The densities and viscosities of the IPA/water mixture solvents with various IPA contents were measured at 25 °C. Fig. 1 shows the variations in the density and viscosity of the mixture solvents against the [IPA]/[IPA + water] wt. ratio. Interestingly, the density and viscosity of the mixture solvents do not change linearly with the IPA/[IPA + water] wt. ratio. The viscosity data show a parabolic curve with maximum viscosity at an [IPA]/[IPA + water] wt. ratio of ~0.55, which corresponds to a [water]/[IPA] molar ratio of ~3/1. Similar viscosity data from the binary mixture of water and alcohol had also been reported by Nagasawa et al. [45], Gonzalez et al. [46], and Li et al. [47]. Water and alcohol are polar compounds; thus, the self-association and inter-molecular association through the hydrogen bonding of these two compounds may have great

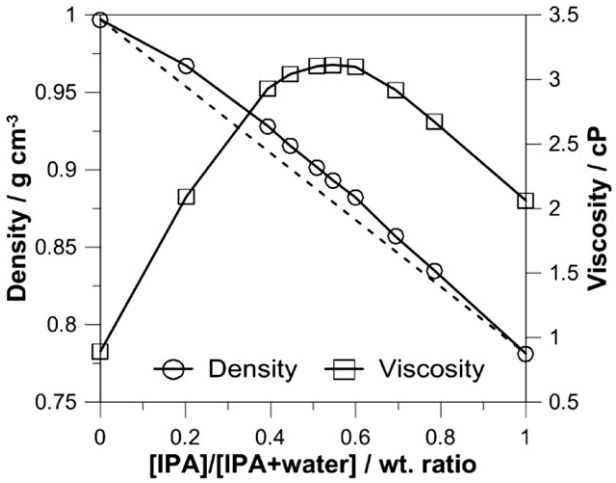

Fig. 1. Density (○) and viscosity (□) of the IPA/water mixture solvents vs. IPA/[IPA + water] wt. ratio at 25 °C. The dashed line indicates the density data calculated from the linear combination of densities of the pure IPA and pure water.

influences on the viscosity and density of the mixture solvents. The density and viscosity data suggest that there is a strong hydrogen bonding interaction between the IPA and water molecules, which leads to mixture solvent densities and viscosities larger than those calculated from the linear combinations of the pure IPA and pure water densities and viscosities, respectively. The maximum number of water molecules bound on each IPA molecule is around 3, i.e., the water/IPA molar ratio is around 3/1 (Fig. 2). Nagasawa et al. [45] suggested that the alcohol molecule is caged inside the H-bond network of water molecules at a water/alcohol molar ratio higher than that of the maximum viscosity and density (i.e., [water]/[IPA] > 3/1 molar ratio). As the alcohol content of the alcohol/water mixture solvent becomes higher than that at the maximum viscosity and density (i.e., [water]/[IPA] < 3/1 molar ratio), alcohol clusters start to form and break the water H-bond network structure, leading to lower viscosity for the mixture solvents with an alcohol fraction higher than that at the maximum viscosity and density.

3.2. TEM and DLS studies of the dilute Nafion-IPA/water solutions

The dilute Nafion IPA/water solutions were frozen at −190 °C and then dried under vacuum at −130 °C on the surface of the TEM copper grid sample holder to fix the conformations of the Nafion molecules similarly to those in the dilute solutions. Fig. 3 shows the TEM micrographs (magnitude 2×10^4) of the Nafion molecular morphology frozen from the 0.6 mg mL^{-1} Nafion IPA/water solutions containing various concentrations of IPA; higher magnitude (1×10^5) TEM micrographs of Nafion IPA/water solutions containing 20, 55, and 80 wt.% IPA are also shown in Fig. 3. These TEM micrographs clearly show that there are small, compact primary Nafion particles in the solutions. When the IPA concentration of the IPA/water mixture solvent is in the range of 20–70 wt.%, these small, compact particles have rod-like structures with rod lengths of around 30–150 nm and tend to aggregate to form larger loose secondary clusters with sizes of around 100–300 nm (Fig. 3a–c and a′). However, the structure of the small, compact particles changes from rod-like to coil-like, and the particle number and size of the loose secondary aggregated clusters decrease as the IPA concentration of the IPA/water mixture solvent is increased from 70 wt.% to 100 wt.% (Fig. 3g–i and h′). The sizes (or rod lengths) of the primary compact particles increase from ~30 nm to ~150 nm as the IPA concentration of the mixture solvent increases from 20 wt.% to 55 wt.% and then decrease from ~150 nm to ~20 nm as the IPA concentration of the IPA/water mixture solvent increases from ~55 wt.% to 100 wt.%. The micrographs also show that the sizes of the loose secondary aggregated clusters and the number of small, compact primary particles within each loose secondary cluster decrease with the increasing IPA concentration of the mixture solvents.

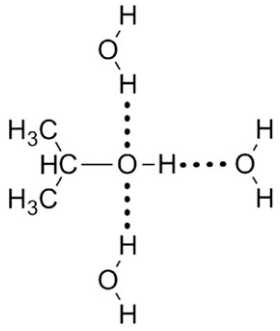

Fig. 2. The hydrogen bonding interactions (i.e., the dotted lines in the graph) between the water and IPA molecules. Each IPA molecule is bound by 3 water molecules when the [water]/[IPA] mole ratio of the mixture solvent is larger than 3/1.

The morphology of Nafion molecules in dilute IPA/water solutions was further investigated using DLS. Fig. 4 illustrates the DLS hydrodynamic radius (i.e., R_h) distributions of the Nafion molecules in various IPA/water mixture solutions and shows two modes of Nafion particle size distributions. Because DLS observes the Nafion particles in solutions, in which the particles are swollen with solvents, and TEM observes the Nafion particles in a dry state without solvents, the sizes of the Nafion particles observed under DLS are larger than those observed under TEM. The DLS small particle mode has R_hs of less than 100 nm, which corresponds to the small, compact primary particles observed in the TEM micrographs. The R_hs of these small primary particles increase when the IPA concentration of the IPA/water mixture solvents is increased from 20 wt.% to 55 wt.% and then decrease when the IPA concentration is increased from 55 wt.% to 100 wt.%. The DLS large particle mode has a R_h distribution of around 100–400 nm, which corresponds to the Nafion large loose secondary aggregated clusters observed in the TEM micrographs. The sizes of these large secondary clusters decrease when the IPA concentration of the IPA/water mixture solvent is increased. These results are similar to those observed in the TEM micrographs (Fig. 3).

3.3. Nafion molecular morphology in dilute IPA/water solutions

In this section, we discuss the Nafion molecular morphology in dilute IPA/water solutions containing various IPA/water compositions. The discussion is based on the δs, εs, and the densities and viscosities of the mixture solvents shown in Section 3.1.

3.3.1. Solubility parameters and dielectric constants

The two chemical compositions of Nafion, i.e., hydrophobic perfluorocarbon backbone (δ_1 = 9.7 $cal^{0.5}$ $cm^{-1.5}$) and hydrophilic sulfonated vinylether side chains (δ_2 = 17.3 $cal^{0.5}$ $cm^{-1.5}$), are incompatible. The variations in the Nafion molecular morphology in dilute solutions observed in TEM and DLS studies can be explained using the δ, ε, and inter IPA-water molecular hydrogen bonding interaction in the solutions. Since the Nafion fluorocarbon backbones and vinylether sulfonic acid side chains are not compatible, the aggregation of Nafion molecules and the formation of compact primary aggregated particles in the solutions cannot be attributed to their interactions but rather to associations

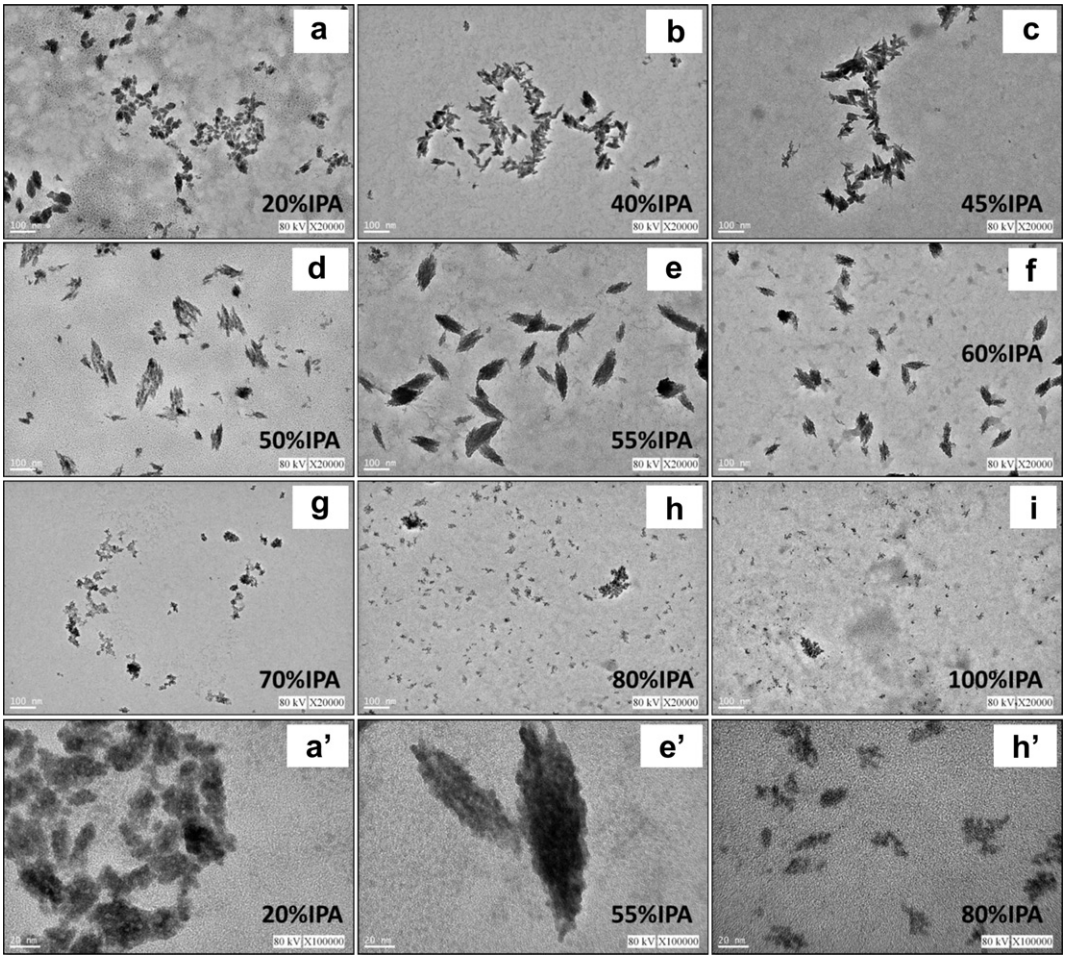

Fig. 3. TEM micrographs (a–i, magnitude 2×10^4, scale bar 100 nm; a′, e′, and h′, magnitude $\times 10^5$, scale bar 20 nm) of Nafion molecular morphology of 0.6 mg mL^{-1} Nafion in IPA/water solutions after freeze drying. The wt.% of IPA in the IPA/water mixture solvents is indicated in each micrograph.

either via the inter-polymer fluorocarbon backbone interactions or via the inter-ionic interactions of two polymer side chain negatively charged $-SO_3^-$ groups with positively charged H_3O^+ ions, i.e., $\sim SO_3^- \cdots [H_3^+O] \cdots {}^-O_3S \sim$. Because of the negative charge repulsion of the side chain vinylether $-SO_3^-$ groups, the inter-polymer fluorocarbon backbone associations dominate the formation of Nafion compact primary aggregated particles, which depends on the compatibility of the solvent with the Nafion fluorocarbon backbones. The less compatible the solvent is with the Nafion fluorocarbon backbones, the larger the primary aggregated particles. The association of the Nafion fluorocarbon backbones in the solutions causes the fluorocarbon backbones to be located within the primary aggregated particles with the negatively charged vinylether sulfonate chains surrounding around the surfaces of the primary aggregated particles [11,12]. Thus, the inter-polymer vinylether sulfonate interactions, i.e., $\sim SO_3^- \cdots [H_3^+O] \cdots {}^-O_3S \sim$, dominate the associations of the compact primary particles and the formation of the loose secondary clusters. The inter-polymer vinylether sulfonate side chain interactions depend on the compatibility of the solvent with the vinylether sulfonate side chains and on the ε of the solvent, which determines the degree of dissociation of the $-SO_3H$ groups and thus the negative charge content of each Nafion compact primary aggregated particle.

The compatibility of the solvent with the Nafion fluorocarbon backbones and the vinylether sulfonate side chains depend on the differences between the δ of the solvent (i.e., δ_s) and the δ_1 of the perfluorocarbon backbones (i.e., $|\delta_s - \delta_1|$) and between the δ_s and the δ_2 of the vinylether sulfonate side chains (i.e., $|\delta_s - \delta_2|$), respectively. The differences $|\delta_s - \delta_1|$ and $|\delta_s - \delta_2|$ are indicators of the compatibility of the solvent with the fluorocarbon backbones and the vinylether sulfonate side chains, respectively. The smaller difference $|\delta_s - \delta|$ indicates higher compatibility of the solvent with the polymer. Table 1 summarizes the dual solubility parameters δ_1 and δ_2 of Nafion [41], and the δ_s and ε of the IPA/water mixture solvents, which were calculated from Eqs. (2) and (3), respectively [18,48,49].

$$\delta_m = \left[E_{coh,m}/V_m\right]^{1/2} = \left[\left(\sum X_i E_{coh,i}\right) \Big/ \left(\sum X_i V_i\right)\right]^{1/2} \quad (2)$$

$$\rho_m = \sum X_i \rho_i = \sum X_i \varepsilon_i^{1/2} M_i \quad (3\text{-a})$$

$$\varepsilon_m = \left[\rho_m \Big/ \sum (X_i M_i)\right]^2 \quad (3\text{-b})$$

In Eqs. (2) and (3), δ_m is the solubility parameter of the mixture solvent, $E_{coh,m}$ the cohesive energy of the mixture solvent, V_m the molar volume of the mixture solvent, X_i the molar ratio of solvent-i, $E_{coh,i}$ the cohesive energy of solvent-i, V_i the molar volume of solvent-i, ρ_m the molar dielectric polarization of a mixture solvent, ρ_i the molar dielectric polarization of solvent-i, ε_m the dielectric constant of a mixture solvent, ε_i the dielectric of solvent-i, and M_i the molecular weight of solvent-i.

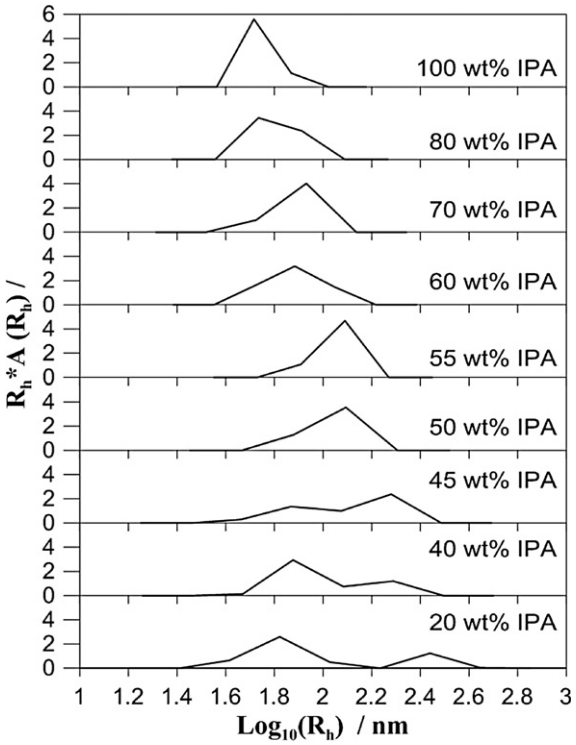

Fig. 4. DLS hydrodynamic radius (R_h) for 0.6 mg mL^{-1} Nafion solutions in IPA/water mixture solvents. Temp = 25 °C, and scattering angle $\theta = 60°$. The numerical values in the figure indicate wt.% of IPA in the mixture solutions.

3.3.2. Intermolecular interaction of IPA and water

Another factor controlling the morphology of Nafion molecules in dilute solutions is the hydrogen bonding interaction between the alcohol and water molecules. As described in Section 3.1 and Fig. 2, each IPA molecule forms a cluster via hydrogen bonding with 3 water molecules inside the cage of the H-bond network of water molecules when the water/IPA molar ratio in the mixture solvent is larger than 3/1. As the water/IPA molar ratio of the mixture solvent is decreased to less than 3/1 (i.e., [IPA]/[IPA + water] > 52.6 wt.%), the IPA molecules start to break the water H-bond network structure and have the chance to form IPA–IPA intermolecular hydrogen bonds. There are excess free water molecules not bound to the IPA molecule in the mixture solvents when the water/IPA molar ratio of the mixture solvent is larger than 3/1 (i.e., [IPA]/[IPA + water] < 52.6 wt.%). These excess H_2O molecules form H_3O^+ ions by bonding with the H^+ ions dissociated from the Nafion side chain $-SO_3H$ groups. The H_3O^+ ion plays an important role in the formation of Nafion secondary ionic cluster aggregations via ionic interaction, i.e., $\sim SO_3^-\cdots[H_3^+O]\cdots{}^-O_3S\sim$. The IPA (i.e., $(CH_3)_2CHOH$) molecules may interact with H^+ ions and form $(CH_3)_2CH{-}OH_2^+$ ions. However, because of the low compatibility of IPA ($\delta_s = 11.8$ cal$^{0.5}$ cm$^{-1.5}$) with the Nafion vinylether sulfonic acid side chains ($\delta_2 = 17.3$ cal$^{0.5}$ cm$^{-1.5}$) and the low ε value of IPA, the probability of the $-SO_3H$ groups to dissociate and form $-SO_3^-$ and H^+ ions is much lower in the $(CH_3)_2CHOH$ environment than in the H_2O environment. The larger steric hindrance of the $[(CH_3)_2CHOH_2^+]$ ions than the $[H_3^+O]$ ions also causes lower interactions of the Nafion $-SO_3^-$ groups with the $[(CH_3)_2CHOH_2^+]$ ions than with the $[H_3^+O]$ ions. Thus, most of the Nafion compact primary aggregated particles associate and form secondary ionic clusters via $-SO_3^-\cdots[H_3^+O]\cdots{}^-O_3S-$ ionic interactions rather than via $-SO_3^-\cdots[(CH_3)_2CHOH_2^+]\cdots{}^-O_3S-$ ionic interactions.

Table 1
The calculated δ and ε of IPA/water mixture solvents.

[IPA]/[IPA + water] (wt.%)	[Water]/[IPA] (molar ratio)	δ_s (cal$^{0.5}$ cm$^{-1.5}$)	ε
Pure water	1/0	23.4	78.4
20	13.3/1	21.2	63.6
40	5/1	19.0	50.4
45	4.1/1	18.5	47.3
50	3.3/1	17.9	44.3
55	2.7/1	17.4	41.5
60	2.2/1	16.8	38.7
70	1.4/1	15.6	33.4
80	0.83/1	14.4	28.5
Pure IPA	0/1	11.8	19.9
Nafion		$\delta_1 = 9.7$ (backbone) $\delta_2 = 17.3$ (side chain)	

3.3.3. Nafion molecular morphology in dilute IPA/water solutions

Since, in the mixture solvent, the maximum number of H_2O molecules bound to one IPA molecule through hydrogen bonding is around 3, we begin the discussion on Nafion solution properties with the IPA/water mixture solvents with $[H_2O]/[IPA]$ molar ratios of ~2.2/1–3.3/1 (i.e., [IPA]/[IPA + water] = 50–60 wt.%). Then we move to the solutions with $[H_2O]/[IPA]$ molar ratios larger than 3.3/1 (i.e., [IPA]/[IPA + water] = 20–45 wt.%). Subsequently, we discuss the solutions with $[H_2O]/[IPA]$ molar ratios lower than 2.2/1 (i.e., [IPA]/[IPA + water] ≧ 70 wt.%).

Table 1 shows that the mixture solvent containing 55 wt.% IPA has a $\delta_s = 17.4$ cal$^{0.5}$ cm$^{-1.5}$, which is close to the value of $\delta_2 = 17.3$ cal$^{0.5}$ cm$^{-1.5}$ and far from that of the $\delta_1 = 9.7$ cal$^{0.5}$ cm$^{-1.5}$ of Nafion, suggesting that this solvent is more compatible with the vinylether side chains rather than with the perfluorocarbon backbones. Thus, in this solvent, Nafion molecules aggregate and form the primary aggregated particles via inter-polymer perfluorocarbon backbone associations with the vinylether side chains surrounding the surfaces of the aggregated particles and in contact with the solvents. The high ε ($\varepsilon = 41.5$) value of this mixture solvent causes high dissociation of the side chain $-SO_3H$ groups to form negatively charged $-SO_3^-$ groups on the surfaces of the aggregated Nafion particles, which lead the primary aggregated particles to form rod-like structures (Fig. 3e and e′). When the IPA concentration of the mixture solvent is decreased to 50 wt.%, the δ_s and ε of the solvent are slightly higher than those of the solvent containing 55 wt.% IPA and the Nafion molecules in this solvent have similar rod-like structure as those in the solvent containing 55 wt.% IPA. However, the higher ε value of the solvent causes the Nafion molecules in this solvent to have more negatively charged $-SO_3^-$ groups dissociated from $-SO_3H$ groups and higher Nafion inter-polymer negative charge repulsions than in the solvent containing 55 wt.% IPA. Thus the Nafion molecules in the solvent containing 50 wt.% IPA have smaller primary aggregations than in the solvent containing 55 wt.% IPA (Fig. 3d and e). As the IPA concentration of the mixture solvent is increased to 60 wt.%, the δ_s and ε of this solvent are slightly lower than those of the mixture solvent containing 55 wt.% of IPA. The TEM micrographs (Fig. 3f and e) and DLS data (Fig. 4) show that the Nafion primary aggregated particles in this solvent have structure similar to but with sizes smaller than those in the solvent containing 55 wt.% of IPA. The smaller Nafion primary aggregated particle sizes in this solvent than in the solvent containing 55 wt.% IPA can be attributed to the smaller difference $|\delta_s - \delta_1|$ of Nafion in this solvent than in the solvent containing 55 wt.% IPA, which leads the Nafion perfluorocarbon backbones to be more compatible with the solvent containing 60 wt.% IPA; thus, smaller primary aggregations in the solvent containing 60 wt.% IPA.

As the IPA concentration of the mixture solvents decreases from 50 wt.% to 20 wt.%, more and more free water molecules not bound

to the IPA molecule appear in the solution. The δ_s and ε of the mixture solvent increase from $\delta_s = 17.9$–21.2 cal$^{0.5}$ cm$^{-1.5}$ and from $\varepsilon = 44.3$ to 63.6, respectively. The difference $|\delta_s - \delta_1|$ is larger than the difference $|\delta_s - \delta_2|$, suggesting that the solvent is more compatible with the Nafion vinylether sulfonic acid side chains than with the perfluorocarbon backbones. The high ε values of the mixture solvents also cause the large formation of negatively charged $-SO_3^-$ groups. Thus, the Nafion molecules aggregate and form primary aggregated rod-like structures, as shown in the TEM micrographs (Fig. 3a–c). However, the increase in the ε value of the mixture solvents also causes an increase in the Nafion inter-polymer $-SO_3^-$ negative charge repulsions, leading to a reduction in the Nafion primary aggregations when the IPA concentration of the IPA/water solvent is decreased, as shown in the TEM and DLS observations (Fig. 4). The decrease of the IPA concentration of the mixture solvent results in an increase in the free water molecules not bound to the IPA, leading to an increase in the $[H_3^+O]$ ions, which facilitate the Nafion primary aggregated particles to proceed to secondary ionic aggregations via the $\sim SO_3^- \cdots [H_3^+O] \cdots {}^-O_3S \sim$ ionic interaction. Thus, the number of Nafion compact primary aggregated particles within each Nafion loose secondary ionic aggregated cluster increases with the decreasing IPA concentration of the solvents, as shown in the TEM and DLS observations.

As the IPA concentration of the mixture solvents increases from 60 wt.% to 100 wt.%, more and more IPA molecules break out from the water H-bond network structure to form IPA–IPA intermolecular hydrogen bonds with no excess free water molecules appearing in the mixture solvents. When the solvent is a pure IPA solvent, the $\delta_s = 11.8$ cal$^{0.5}$ cm$^{-1.5}$ is close to the δ_1 of Nafion and the difference $|\delta_s - \delta_1|$ is smaller than $|\delta_s - \delta_2|$, indicating the pure IPA solvent is more compatible with the perfluorocarbon backbones than with the vinylether sulfonic acid side chains. The Nafion molecules form primary coiled particles with the perfluorocarbon backbones in contact with the IPA solvent and the vinylether sulfonic acid side chains buried inside the coiled structures, as shown in the TEM micrograph (Fig. 3i). The low ε value of the IPA causes a low dissociation of the Nafion $-SO_3H$ groups and thus low negatively charged $-SO_3^-$ groups on the polymer chains. Few secondary ionic aggregated clusters and primary rod-like Nafion aggregated particles appear in the pure IPA solvent.

For mixture solvents with the IPA concentration of ~70–80 wt.%, which is in a solvent region between the maximum solvent viscosity ($[H_2O]/[IPA] = \sim 2.2/1$–$3.3/1$ molar ratio) and the pure IPA solvent, the difference $|\delta_s - \delta_1|$ decreases with increasing the IPA concentration of the mixture solvent. As the IPA concentration of the mixture solvent is near 70 wt.%, the difference $|\delta_s - \delta_1|$ is still larger than $|\delta_s - \delta_2|$; the Nafion molecules aggregate via perfluorocarbon backbone associations to form primary aggregated particles. However, the low ε value of this solvent causes a low negatively charged $-SO_3^-$ groups forming on the polymer chains. Few rigid rod-like Nafion particles are observed in this solvent (Fig. 3g). When the IPA concentration of the mixture solvent is close to 80 wt.%, which means there are more IPA molecules than water molecules, the Nafion molecules have a greater chance of coming in contact with IPA molecules than with water molecules, leading the conformation of the Nafion molecules to be similar to that of Nafion molecules in the pure IPA solvent (a coiled structure conformation as shown in the TEM micrographs (Fig. 3h and h′). TEM (Fig. 3g and h) and DLS (Fig. 4) studies show that the size of the Nafion primary aggregated particles decreases with the increasing IPA concentration of the mixture solvent from 70 to 80 wt.% and is smaller than that in the mixture solvents containing less than 70 wt.% of IPA, due to the better compatibility of the Nafion perfluorocarbon backbones with the solvent having a higher IPA content. The low negatively charged $-SO_3^-$ group content on the polymer chains, also retards the formation of secondary ionic aggregations. Thus, few secondary ionic aggregated clusters are observed in these solutions as shown in the TEM and DLS observations.

3.4. Pt-ECSAs of the Pt–C/Nafion GDEs

The CL of the GDE consists of Pt–C and Nafion ionomer. The Nafion ionomer extends the Pt three-dimensional reaction zone and increases the catalyst utilization. The presence of the Nafion ionomer aids proton transport in the CLs; however, over-loading of Nafion in the CLs results in high shielding of Pt particles by Nafion ionomer and retards the H_2 and O_2 gases reaching the Pt particles for electrochemical reactions. Several research groups have evaluated the Nafion ionomer content of CLs using CV analyses and fuel cell tests [50,51]. Passalacqua et al. [50] and Qi et al. [51] reported an optimum Nafion content in CLs of around 30–33 wt.%. However, they did not reported on the influence of the solvent of the catalyst ink solutions on the fuel cell performance. In this study, all the catalyst ink solutions were prepared with a fixed [Pt–C]/[Nafion] wt. ratio of 2.3/1 (see Section 2.5). Thus, the Nafion content in the CL of each sample was fixed at ~30 wt.%. The Pt-ECSAs of the Pt–C/Nafion GDEs prepared from IPA/water solutions containing 20–80 wt.% IPA were investigated using CV in deaerated 0.5 M H_2SO_4 solution. Fig. 5 shows the cyclic voltammograms of these electrodes recorded at room temperature. The Pt-ECSA of each sample was calculated from the measuring charges collected in the hydrogen adsorption/desorption region assuming a value of 210 mC cm^{-2} for the adsorption of a hydrogen monolayer [43,44,52]. The calculated Pt-ECSA data of these GDEs were plotted against the [IPA]/[IPA + water] wt. ratio of the mixture solvent of the catalyst ink solutions (Fig. 6a). As shown in the figure, the Pt-ECSA value of the electrode decreases with the increase in the IPA concentration of the mixture solvent and has a plateau region at the [IPA]/[IPA + water] wt. ratio of 0.45–0.60 (i.e., [water]/[IPA] = 4/1–2/1 molar ratio), which corresponds to the maximum viscosity region of the IPA/water mixture solvents, as shown in Fig. 1. The composition of the IPA/water solvents, and thus the morphology of the Nafion molecules in the catalyst ink solutions, clearly has a strong influence on the microstructure of the Nafion thin film of the Pt–C/Nafion CL coating on the surface of the carbon paper GDL. Thus, the Pt-ECSA of a Pt–C/Nafion GDE strongly depends on the solvent

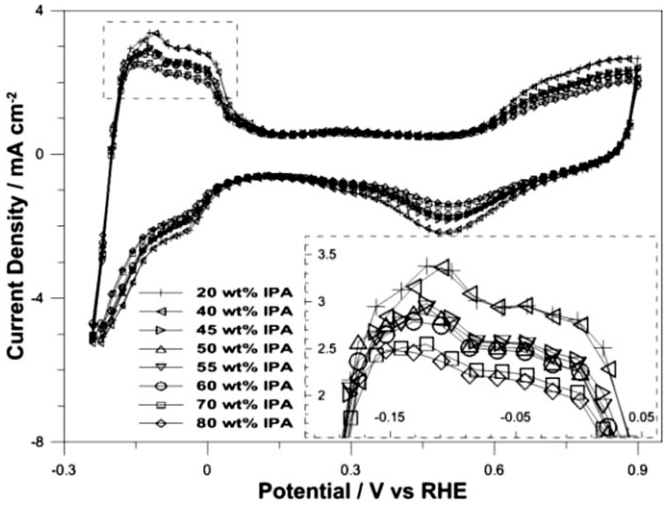

Fig. 5. Cyclic voltammetry (CV) curves of Pt–C/Nafion GDEs prepared from various IPA/water mixture solvents. Wt.% of IPA in the IPA/water mixture solvents: (+) 20 wt.%; (◁) 40 wt.%; (▷) 45 wt.%; (△) 50 wt.%; (▽) 55 wt.%; (○) 60 wt.%; (□) 70 wt.%; (◇) 80 wt.%.

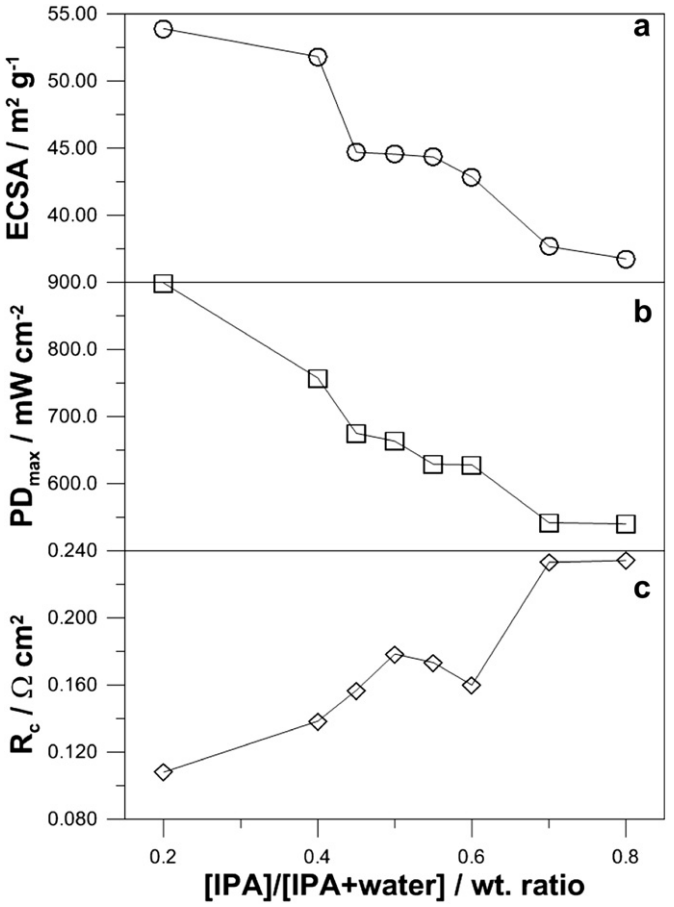

Fig. 6. Plots of: (a) CV test Pt-ECSA data; (b) fuel cell test PD_{max} data; (c) CL impedance R_c data versus the [IPA]/[IPA + water] wt. ratio of the mixture solvents of the Pt–C/Nafion catalyst ink solutions for Pt–C/Nafion GDEs fabrication.

composition of the Pt–C/Nafion catalyst ink solutions for CL fabrication.

3.5. PEMFC unit cell tests and impedance studies of the MEAs

The MEAs prepared from the Nafion-212 membrane with CLs fabricated using IPA/water solvents consisting of various IPA concentrations were used for unit fuel cell performance tests at 80 °C with humidified H_2/O_2 gases. Fig. 7 illustrates the fuel cell test *i*–V curves of these MEAs. The maximum power density (PD_{max}) of each MEA is calculated from its *i*–V data (Table 2) and plotted against the IPA concentration of the IPA/water solvent of the Pt–C/Nafion catalyst ink solutions, as shown in Fig. 6b. The results show that the PD_{max} and Pt-ECSA have the same dependence on the IPA concentration of the IPA/water solvent of the Pt–C/Nafion catalyst ink solution. Both the PD_{max} and Pt-ECSA values decrease with the increasing IPA concentration of the IPA/water mixture solvent and have a plateau region at an IPA concentration of ∼45–60 wt.% of the mixture solvent (i.e., $[H_2O]/[IPA] \sim 3/1$ molar ratio).

AC impedance measurements were also carried out to investigate the resistance of the CLs of the MEAs prepared from various IPA/water mixture solvents. The AC impedance diagrams were simulated using a Randles equivalent circuit consisting of a resistance R_s, representing the total non-electrode cell ohmic resistance in series, with cathode charge transfer resistance R_c, which is parallel with capacitive-like element C_d, representative of the electrode double layer [53]. In a fuel cell, the main contribution to

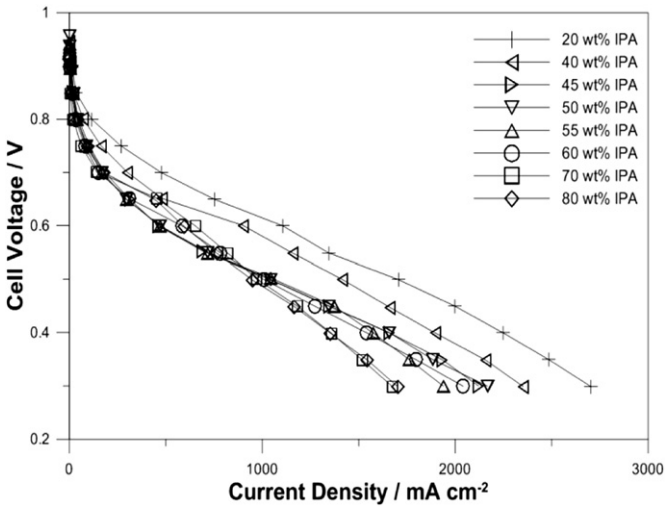

Fig. 7. Polarization curves of PEMFCs with MEAs prepared from catalyst ink solutions containing IPA/water mixture solvents with various IPA concentrations. Wt.% of IPA in the IPA/water mixture solvents: (+) 20 wt.%; (◁) 40 wt.%; (▷) 45 wt.%; (△) 50 wt.%; (▽) 55 wt.%; (○) 60 wt.%; (□) 70 wt.%; (◇) 80 wt.%.

R_s (high frequency resistance) comes from the proton transport resistance of the membrane. Fig. 8 shows the AC impedance diagrams obtained at constant current $i = 1000$ mA cm^{-2} for MEAs with Pt–C/Nafion CLs prepared from IPA/water solvents containing various concentrations of IPA. Table 2 lists the R_s and R_c values in the impedance diagrams simulated using a Randles equivalent circuit. Fig. 8 and Table 2 show that the R_s value does not change significantly with the IPA concentration of the solvents of the Pt–C/Nafion catalyst ink solutions for MEA CL fabrication, because the same membrane (i.e., Nafion-212 membrane) and the same cell and flow field were used in fuel cell tests. The difference in the fuel cell performance of these MEAs mainly comes from the difference in the R_c values of the MEAs. The variation in the R_c value versus the IPA concentration of the IPA/water solvents of the Pt–C/Nafion catalyst ink solution is also given in Fig. 6c, which shows that R_c increases with the increasing IPA concentration of the IPA/water solvent of the catalyst ink solution and has a plateau region at an IPA concentration of ∼45–60 wt.%, which is in consistent with the Pt-ECSA (Fig. 6a) and fuel cell PD_{max} (Fig. 6b) data.

3.6. Morphology of the Pt–C/Nafion layer of the GDEs

All the samples used in CV Pt-ECSA, fuel cell *i*–*V*, and impedance measurements were prepared by ultrasonic spraying of the Pt–C/Nafion catalyst ink solutions on the GDLs, with fixed Pt–C and Nafion loadings. The difference among these samples is in the IPA/water composition of the Pt–C/Nafion catalyst ink solutions used in

Table 2
R_s and R_c impedance and fuel cell test PD_{max} data of the MEAs prepared from IPA/water mixture solvents containing various concentrations of IPA.

[IPA]/[IPA + water] (wt.%)	R_s (Ω cm^2)	R_c (Ω cm^2)	PD_{max} (mW cm^{-2})
20	0.078	0.103	899
40	0.083	0.137	757
45	0.087	0.157	675
50	0.087	0.177	663
55	0.087	0.170	629
60	0.085	0.160	628
70	0.087	0.227	542
80	0.090	0.229	540

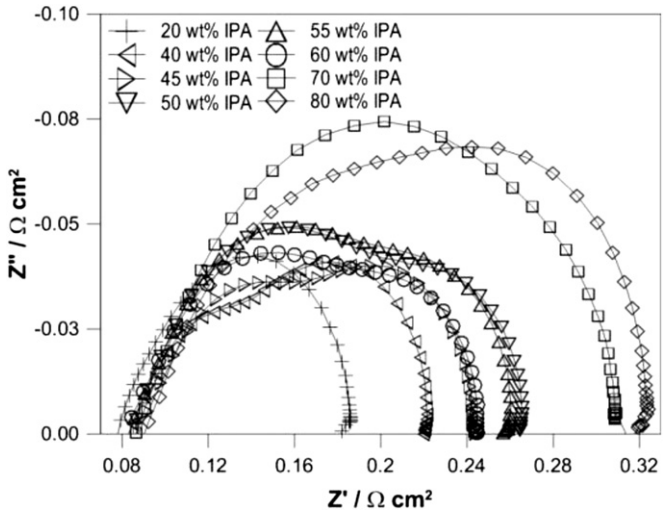

Fig. 8. AC impedance diagrams of MEAs obtained at a constant current $i = 1000$ mA cm^{-2}. The Pt–C/Nafion CLs of the MEAs were prepared from IPA/water mixture solvents containing various concentrations of IPA. Wt.% of IPA in the IPA/water mixture solvents: (+) 20 wt.%; (◁) 40 wt.%; (▷) 45 wt.%; (△) 50 wt.%; (▽) 55 wt.%; (○) 60 wt.%; (□) 70 wt.%; (◇) 80 wt.%.

ultrasonic spraying. The IPA/water composition of the Pt–C/Nafion catalyst ink solutions plays the key role in determining the morphology of the Nafion ionomer thin layer in the CLs and thus the Pt-ECSA, R_c, and PD_{max} of the MEAs. Further investigation of the influence of the composition of the IPA/water solvent of the Pt–C/Nafion catalyst ink solutions on the morphology of the Pt–C/Nafion CLs was carried out using FESEM. The samples used in the FESEM observations were the same as those used in the CV Pt-ECSA studies.

Fig. 9 shows the FESEM micrographs of the Pt–C/Nafion thin layer of the GDE samples, which were prepared from Pt–C/Nafion–IPA/water ink solutions with solvents containing 20–80 wt.% IPA. The micrograph of the Pt–C particles dispersed on GDL surface without the Nafion resin (which was prepared by spraying a layer of Pt–C/acetone solution on the GDL surface and then evaporating the acetone solvent) is also shown in Fig. 9i for reference. These micrographs clearly show the carbon powder supports (gray particles with diameters of ~60–80 nm) with Pt particles (bright spots with diameters of less than 5 nm) dispersed on their surfaces. These micrographs show that the number of visible Pt particles on the surfaces of the carbon powder supports decreases with the increasing IPA concentration of the IPA/water solvents of the Pt–C/Nafion catalyst ink solutions. The number of visible Pt particles of the Pt–C/Nafion GDEs prepared from the solvents containing 20 wt.% IPA (Fig. 9h) is similar to that of the Pt–C particles on the GDL without Nafion (Fig. 9i). However, the number of visible Pt particles decreases as the IPA concentration of the solvent increases from 20 wt.% to 80 wt.% (Fig. 9h–a). Obviously, some of the Pt particles were shielded by the Nafion ionomer layer covering the surfaces of the carbon powder supports and are not visible in the FESEM micrographs. The number of non-visible Pt particles shielded by the Nafion film increases with the increasing IPA concentration of the IPA/water solvents of the Pt–C/Nafion catalyst ink solutions.

The Pt–C/Nafion catalyst ink solutions used in fabricating GDEs for CV and fuel cell tests have a Pt–C/Nafion/[IPA + water] wt. ratio of 2.3/1/327; these are dilute solutions with a Nafion concentration of less than 0.6 mg mL^{-1}. Using the Nafion molecular weight of 2.5×10^5 g mol^{-1} [54] and the carbon powder density of 2.1 g cm^{-3}, we obtained ~940 Nafion polymer chains shared by one Pt–C (Pt content 38 wt.%) particle in the Pt–C/Nafion catalyst ink solution when the Pt–C/Nafion wt. ratio was 2.3/1. Comparing the FESEM micrographs of the Pt–C/Nafion layer on the GDL (Fig. 9) with the TEM micrographs of the Nafion particles frozen from the dilute solutions containing various concentrations of IPA (Fig. 3) and the DLS Nafion particle size R_h distributions in the dilute solutions (Fig. 4), we found that the diameter D of the carbon powder support of a Pt–C particle was smaller than that of the Nafion particles in the IPA/water solutions containing 70–80 wt.% of IPA. When the IPA concentration of the IPA/water solvent is at 50–60 wt.%, the Nafion molecules have rod-like structures with the rod width W shorter than the D of the carbon powder supports and the rod length L longer than the D of the carbon powder supports. When the IPA concentration of the IPA/water solvent decreases from 50 wt.% to 20 wt.%, both the W and L of the Nafion primary rod-like particles decrease, but the degree of the secondary ionic aggregation and the size d of the secondary ionic aggregated clusters increase. The sizes d of the secondary aggregated clusters are larger than the sizes D of the carbon powders. Fig. 10a–c shows the dispersion of Nafion particles on the surfaces of the Pt–C particles in the dilute solutions with the IPA concentrations of the mixture solvents at 70–80 wt.%, 50–60 wt.%, and 20–45 wt.%, respectively. Fig. 10a′–c′ are the Pt–C/Nafion thin layers deposited on the surface of GDLs, which were prepared by ultrasonic spraying the Pt–C/Nafion catalyst ink solutions of Fig. 10a–c, respectively, on the surface of GDLs. In the mixture solvents containing ~70–80 wt.% of IPA, the small, flexible, and low negative charged Nafion particles are easy to disperse and contact on the surface of the carbon powder (Fig. 10a). It is possible that the Pt–C particles are shielded by more than one layer of Nafion ionomer after they are sprayed on the surface of GDL, because of the sharing of 940 Nafion polymers by one Pt–C particle. After the catalyst ink solutions are ultrasonic sprayed and deposited on the surface of GDL, the small, flexible, and low negative charge Nafion particles which are not in touching with Pt–C particles in the solutions (Fig. 10a) smoothly lie down and in contact with the surfaces of the Pt–C particles with few voids appearing between the interface of the Nafion layer and Pt–C particles (Fig. 10a′). Most of the Pt particles on the surfaces of the carbon powders are shielded by the Nafion ionomer for the GDEs prepared using the catalyst ink solutions containing 70–80 wt.% of IPA. However, because of the large steric hindrance and high negative charge of the large Nafion aggregated rigid rod-like particles in the solutions containing 60–20 wt.% IPA, there are obstacles to the deposition of these large, rigid, and highly negatively charged Nafion particles on the surfaces of the Pt–C particles when some rigid and large Nafion aggregated particles have previously been deposited on the Pt–C particle surfaces (Fig. 10b′ and c′). These obstacles increase with the Nafion particle sizes and negative charge content. Fig. 10b′ and c′ shows the large, rigid, and highly negatively charged Nafion particles which are not in contact with the Pt–C particles in the solutions (Fig. 10b and c) lie down and touch the surfaces of the Pt–C particles with large voids appearing between the interface of the Nafion layer and Pt–C particles after the catalyst ink solutions are ultrasonic sprayed and deposited on the surface of GDLs. Thus, the number of Nafion ionomer layers in contact on the surface of the Pt–C particles decreases and the number of the Pt particles not shielded by the Nafion ionomer increases with the decreasing IPA concentration of the IPA/water solvent in the Pt–C/Nafion catalyst ink solutions. Hence, the Pt-ECSA and fuel cell performance increase with the decreasing IPA concentration of the IPA/water solvents of the Pt–C/Nafion catalyst ink solutions for CL fabrications. The increase in fuel cell performance with decreasing IPA concentrations of the IPA/water solvents of the Pt–C/Nafion catalyst ink solutions can also be attributed to the increase in the negatively charged $-SO_3^-$ groups located on the surfaces of the

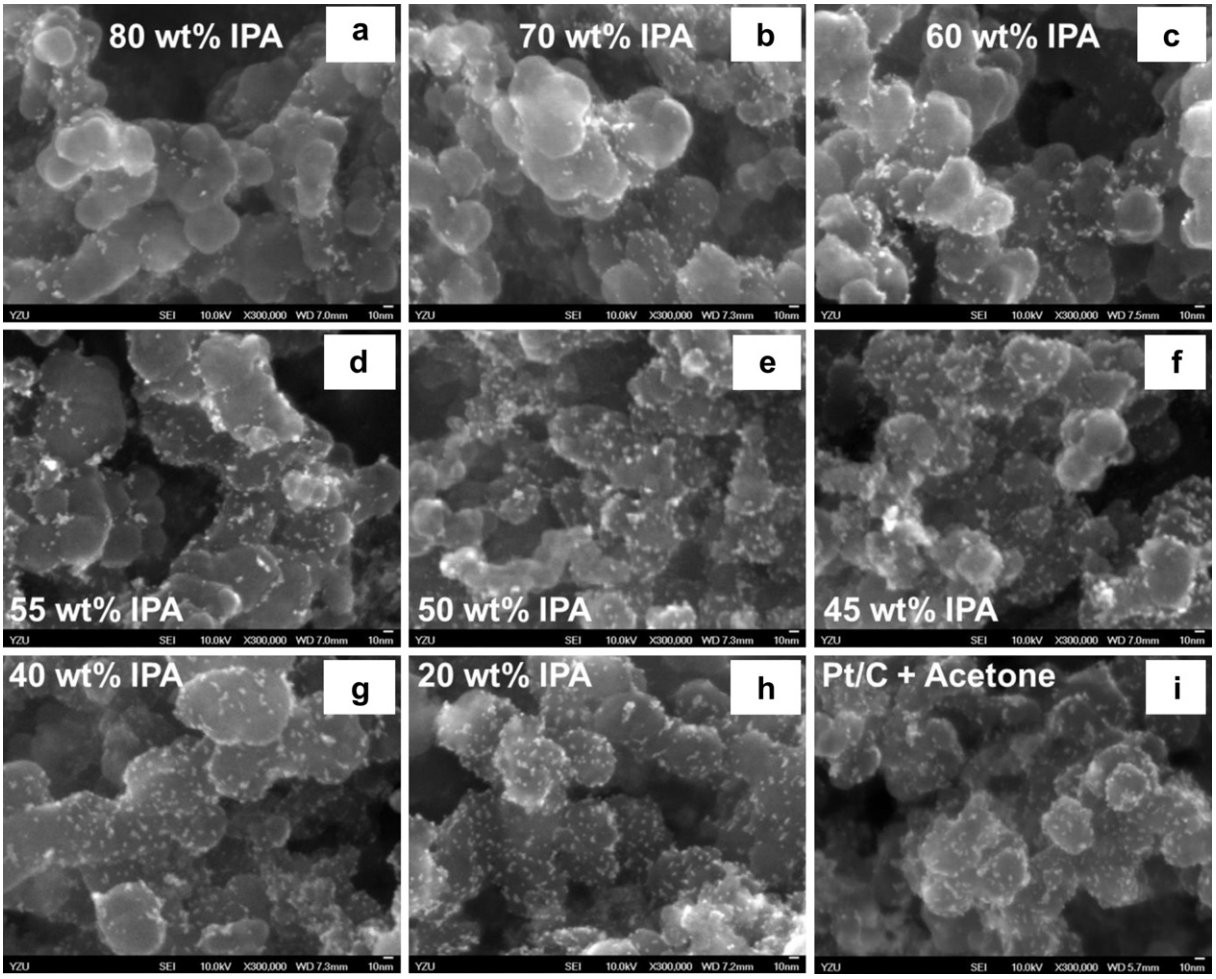

Fig. 9. FESEM micrographs (3×10^5; the scale bar is 10 nm) of the Pt–C/Nafion layer on the surface GDL. [Pt–C]/[Nafion] = 2.3/1 by wt. The gray particles with diameters of ~60–80 nm are carbon powders, and the bright spots with sizes <5 nm are Pt particles. The IPA concentrations of the Pt–C/Nafion catalyst ink solutions for CL fabrications are: (a) 80 wt.%; (b) 70 wt.%; (c) 60 wt.%; (d) 55 wt.%; (e) 50 wt.%; (f) 45 wt.%; (g) 40 wt.%; (h) 20 wt.% IPA; (i) Pt–C on GDL without Nafion.

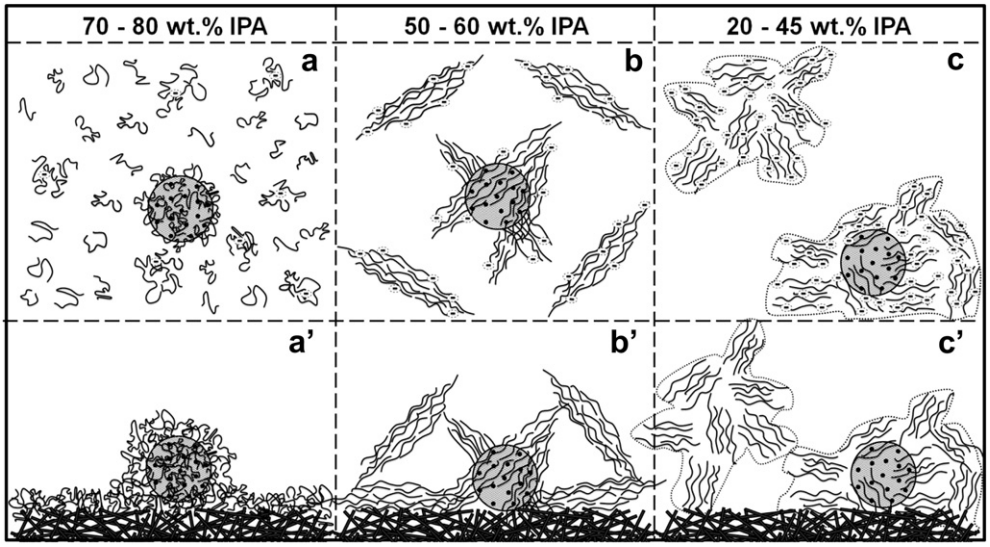

Fig. 10. Top row: the Pt–C/Nafion dilute IPA/water solutions, in which the IPA concentration in the mixture solvents is: (a) 70–80 wt.% IPA; (b) 50–60 wt.% IPA; (c) 20–45 wt.% IPA. Bottom row: the Pt–C/Nafion layer ultrasonic sprayed on the surface of carbon paper GDL after evaporating the solvent. The IPA concentrations of the IPA/water mixture solvents of Pt–C/Nafion catalyst ink solutions used for preparing GDEs are: (a′) 70–80 wt.% IPA; (b′) 50–60 wt.% IPA; (c′) 20–45 wt.% IPA.

Nafion particles as the water concentration of the solvents increases, which raises the possibility for the Pt particles to come in contact with the $-SO_3^-$ groups, thus facilitating the transference of H^+ ions, which are generated from the electrochemical catalytic reaction on the surfaces of Pt particles in the CLs.

4. Conclusions

This study investigated the Nafion molecular morphology in dilute IPA/water solutions containing 20–80 wt.% of IPA and the morphology of the Pt–C/Nafion layer in GDEs using TEM, DLS, and FESEM. The Nafion molecules were found to form primary aggregated particles via inter-fluorocarbon backbone aggregations (20–60 wt.% IPA), and these primary aggregated particles may form secondary ionic clusters via inter-sulfonate ionic aggregations (20–45 wt.% IPA) in dilute IPA/water solutions. The structure of the primary aggregated particles changes from rod-like to coil-like when the IPA concentration of the solvent is above 70 wt.%. Regarding the primary and secondary aggregations, we may conclude that the Nafion aggregated particle sizes in the dilute solutions decrease with the increasing IPA concentration of the IPA/water solvents. The FESEM observations and CV measurements of the GDEs showed that both the number of Pt particles not shielded by Nafion ionomers and the Pt-ECSA of the CLs increased with the decreasing IPA concentration of the IPA/water solvents of the Pt–C/Nafion ink solutions for CL fabrication. The fuel cell tests of the MEAs also showed that the performance increased as the IPA concentration of the IPA/water solvents of the Pt–C/Nafion ink solutions for CL fabrications decreased from 80 wt.% to 20 wt.%. These results suggested that the Pt-ECSA of the CL and the fuel cell performance of the MEA strongly depend on the composition of the IPA/water solvent of the Pt–C/Nafion catalyst ink solutions for CL fabrication. A lower IPA content in the IPA/water solvent of the Pt–C/Nafion catalyst ink solutions results in the formation of larger and higher negatively charged Nafion aggregated particles, which leads to higher steric hindrance and higher charge repulsion of the deposition of Nafion particles on the surface of Pt–C particles and thus a thinner Nafion film in contact on the surfaces of the Pt–C particles. The thinner Nafion film in contact with the Pt particles in the CL of MEAs increases the chances of the Pt particles to come in contact with the input H_2/O_2 fuel gases and thus enhances the generation of H^+ ions on the Pt particle surfaces in the CL, leading to higher fuel cell performance.

Acknowledgments

The authors would like to thank National Science Council (NSC), Taiwan, ROC for the financial support through grant NSC-96-2221-E-155-041-MY3.

References

[1] W.G. Grot, Nafion as a Separator in Electrolyte Cells, In: Nafion Product Bulletin, DE, Du Pont Co, Wilmington, DE, 1986.
[2] W.G. Grot, US Patent 4, 453, 991, 1986.
[3] R.B. Moore, C.R. Martin, Anal. Chem. 58 (1986) 2569–2571.
[4] R.B. Moore, C.R. Martin, Macromolecules 21 (1988) 1334–1339.
[5] E.J. Taylor, E.B. Anderson, N.R.K. Vilambi, J. Electrochem. Soc. 139 (1992) L45–L46.
[6] X. Ren, M.S. Wilson, S. Gottesfeld, J. Electrochem. Soc. 143 (1996) L12–L15.
[7] Z. Xie, T. Navessin, X. Zhao, M. Adachi, S. Holdcroft, T. Mashio, A. Ohma, K. Shinohara, ECS Trans. 16 (2008) 1811–1816.
[8] P. Aldebert, G. Gebel, B. Loppinet, N. Nakamura, Polymer 36 (1995) 431–434.
[9] P. Aldebert, B. Dreyfus, M. Pineri, Macromolecules 19 (1986) 2651–2653.
[10] B. Loppinet, G. Gebel, C.E. Williams, J. Phys. Chem. B 101 (1997) 1884–1892.
[11] E. Szajdzinska-Pietek, S. Schlick, Langmuir 10 (1994) 1101–1109.
[12] E. Szajdzinska-Pietek, S. Schlick, Langmuir 10 (1994) 2188–2196.
[13] H. Li, S. Schlick, Polymer 36 (1995) 1141–1146.
[14] P.A. Cirkel, T. Okada, S. Kinugasa, Macromolecules 32 (1999) 531–533.
[15] S. Jiang, K.Q. Xia, G. Xu, Macromolecules 34 (2001) 7783–7788.
[16] S.J. Lee, T.L. Yu, H.L. Lin, W.H. Liu, C.L. Lai, Polymer 45 (2004) 2853–2862.
[17] H.L. Lin, T.L. Yu, C.H. Huang, T.L. Lin, J. Polym. Sci. Part. B Polym. Phys. 43 (2005) 3044–3057.
[18] C.H. Ma, T.L. Yu, H.L. Lin, Y.T. Huang, Y.L. Chen, U.S. Jeng, Y.H. Lai, Y.S. Sun, Polymer 50 (2009) 1764–1777.
[19] E.J. Roche, M. Pineri, R. Duplessix, A.M. Levelut, J. Polym. Sci. Part. B Polym. Phys. 19 (1981) 1–11.
[20] T.D. Gierke, G.E. Munn, F.C. Wilson, J. Polym. Sci. Part. B Polym. Phys. 19 (1981) 1687–1704.
[21] M. Fujimura, T. Hashimoto, H. Kawai, Macromolecules 14 (1981) 1309–1315.
[22] M. Fujimura, T. Hashimoto, H. Kawai, Macromolecules 14 (1982) 136–144.
[23] S. Kumar, M. Pineri, J. Polym. Sci. Polym. Phys. Ed. 24 (1986) 1767–1782.
[24] J. Halim, G.G. Scherer, M. Stamm, Macromol. Chem. Phys. 195 (1994) 3783–3788.
[25] J.A. Elliot, S. Hanna, A.M.S. Elliot, G.E. Cooley, Macromolecules 33 (2000) 4161–4171.
[26] G. Gebel, J. Lambard, Macromolecules 30 (1997) 7914–7920.
[27] G. Gebel, Polymer 41 (2000) 5829–5838.
[28] H.W. Starkweather, Macromolecules 15 (1982) 320–323.
[29] M.H. Litt, Polym. Prepr. (Am. Chem. Soc. Div. Polym. Chem.) 38 (1997) 80–81.
[30] L. Rubatat, A.L. Rollet, G. Gebel, O. Diat, Macromolecules 35 (2002) 4050–4055.
[31] L. Rubatat, G. Gebel, O. Diat, Macromolecules 37 (2004) 7772–7783.
[32] M.S. Wilson, S. Gottsfeld, J. Appl. Electrochem. 22 (1992) 1–7.
[33] M. Uchida, Y. Fukuoka, Y. Sugawara, H. Ohara, A. Ohta, J. Electrochem. Soc. 145 (1998) 3708–3713.
[34] M.S. Wilson, J.A. Valerio, S. Gottesfeld, Electrochim. Acta 40 (1995) 355–363.
[35] S.J. Shin, J.K. Lee, H.Y. Ha, S.A. Hong, H.S. Chun, I.H. Oh, J. Power Sources 106 (2002) 146–152.
[36] T.H. Yang, Y.G. Yoon, G.G. Park, W.Y. Lee, C.S. Kim, J. Power Sources 127 (2004) 230–233.
[37] M. Chisaka, E. Matsuoka, H. Daiguji, J. Electrochem. Soc. 157 (2010) B1218–B1221.
[38] R. Fernandez, P. Ferreira-Aparicio, L. Daza, J. Power Sources 151 (2005) 18–24.
[39] D.C. Huang, P.J. Yu, F.J. Liu, S.L. Huang, K.L. Hsueh, Y.C. Chen, C.H. Wu, W.C. Chang, F.H. Tsau, Int. J. Electrochem. Sci. 6 (2011) 2551–2565.
[40] A. Therdthianwong, P. Ekdharmasuit, S. Therdthianwong, Energy Fuels 24 (2010) 1191–1196.
[41] R. Yeo, Polymer 21 (1980) 432–435.
[42] J.A. Dean, Lange's Handbook of Chemistry, thirteenth ed,, McGraw-Hill Book Co., New York, 1987 (Chapter 10).
[43] T.J. Schmidt, H.A. Gasteiger, G.D. Stab, P.M. Urban, D.M. Kolb, R.J. Behm, J. Electrochem. Soc. 145 (1998) 2354–2358.
[44] L. Colombi Ciacchi, A. De Vita, J. Phys. Chem. B 107 (2003) 1755–1764.
[45] Y. Nagasawa, Y. Nakagawa, A. Nagafuji, T. Okada, H. Miyasaka, J. Mol. Struct. 735–736 (2005) 217–223.
[46] B. Gonzalez, N. Calvar, E. Gomez, A. Dominguez, J. Chem. Thermodyn. 39 (2007) 1578–1588.
[47] X. Li, G. Xu, Y. Wang, Y. Hu, Chin. J. Chem. Eng. 17 (2009) 1009–1013.
[48] E.A. Grulke, in: J. Brandrup, E.H. Immergut (Eds.), Polymer Handbook, third ed., Wiley Interscience, 1989, pp. VII/519–VII/559.
[49] D.W. Van Krevelen, P.S. Hoftyzer, Properties of Polymers, Elsevier, 1976 (Chapter 7).
[50] E. Passalacqua, F. Lufrano, G. Squadrito, A. Pattis, L. Giorgi, Electrochim. Acta 46 (2001) 799–805.
[51] Z. Qi, A. Kaufman, J. Power Sources 113 (2003) 37–43.
[52] D. He, C. Zeng, C. Xu, N. Cheng, H. Li, S. Mu, M. Pan, Langmuir 27 (2011) 5582–5588.
[53] K.R. Cooper, V. Ramani, J.M. Fenton, H.R. Kunz, Experimental Methods and Data Analyses for Polymer Electrolyte Fuel Cells, Scribner Associates, Inc, North Carolina, 2006, Laboratory #5 – Impedance spectroscopy of PEM fuel cells.
[54] W.H. Liu, T.Y. Yu, T.L. Yu, H.L. Lin, e-Polymers 109 (2007) 1–8.